Applied Surface Science 344 (2015) 1–8

Contents lists available at ScienceDirect

Applied Surface Science

journal homepage: www.elsevier.com/locate/apsusc

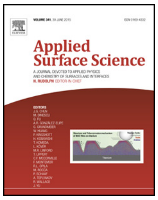

Effect of powder reactivity on fabrication and properties of NiAl/Al_2O_3 composite coated on cast iron using spark plasma sintering

Maryam Beyhaghi[a], Ali-Reza Kiani-Rashid[a,*], Mehrdad Kashefi[a], Jalil Vahdati Khaki[a], Stefan Jonsson[b]

[a] Department of Metallurgical and Materials Engineering, Ferdowsi University of Mashhad, 91775-1111 Mashhad, Iran
[b] Department of Materials Science and Engineering, Royal institute of Technology, SE-10044 Stockholm, Sweden

ARTICLE INFO

Article history:
Received 5 September 2014
Received in revised form 2 January 2015
Accepted 24 January 2015
Available online 3 February 2015

Keywords:
Coatings
Composites
Mechanical activation
Spark plasma sintering
NiAl
Al_2O_3

ABSTRACT

Powder mixtures of Ni, NiO and Al are ball milled for 1 and 10 h. X-ray diffractometry and differential thermal analysis show that while ball milling for 1 h produced mechanically activated powder; 10 h ball milling produced NiAl and Al_2O_3 phases. Dense NiAl/Al_2O_3 composite coatings are formed on gray cast iron substrate by spark plasma sintering (SPS) technique. The effect of powder reactivity on microstructure, hardness and scratch hardness of NiAl/Al_2O_3 coatings after SPS is discussed. Results show that in the coating sample made of mechanically activated powder *in situ* synthesis of NiAl/Al_2O_3 composite coating is fulfilled and a thicker well-formed diffusion bond layer at the interface between coating and substrate is observed. The diffusion of elements across the bond layers and phase evolution in the bond layers were investigated. No pores or cracks were observed at the interface between coating layer and substrate in any of samples. Higher Vickers hardness and scratch hardness values in coating made of 10 h ball milled powder than in coating fabricated from 1 h ball milled powder are attributed to better dispersion of Al_2O_3 reinforcement particles in NiAl matrix and nano-crystalline structure of NiAl matrix. Scratched surface of coatings did not reveal any cracking or spallation at coating-substrate interface indicating their good adherence at test conditions.

1. Introduction

Intermetallics, such as nickel aluminides, are well known because of their high melting temperature, relatively low density, good oxidation and corrosion resistance [1]. Furthermore, to improve their hardness, strength, creep and wear resistance the addition of reinforcements to matrix of the intermetallics is also important [2]. Among different methods, *in situ* reinforcement has some benefits such as the production of clean interfaces resulting in stronger binding with matrix as well as in thermodynamic stability and uniform dispersion [3]. Alumina has been suggested as a good reinforcement candidate for NiAl intermetallic [4]; and NiAl–Al_2O_3 composite is considered as a promising composite for high temperature applications by improved oxidation resistance [5]. In addition, dispersed particles that act as obstacles to the dislocation motion and prevent grain boundary sliding can also improve creep resistance [6].

Applying intermetallic compounds like Ni–Al coatings on metals can improve their surface properties and enlarge the range of their use [7]. Also, NiAl can be used as a bond coat in thermal barrier coating systems in high temperature oxidizing conditions [8]. To achieve durable coatings, it is very important to attain a strong and resistant bond to the substrate. To promote bonding, a supplementary interface bond layer should exist [9]. Sierra and Vázquez [10] used solar energy concentrated by a Fresnel lens to ignite a self-propagating high-temperature synthesis in a powder mixture of nickel–aluminum to fabricate NiAl coatings on a carbon steel substrate. While they achieved NiAl coating, microstructural observations revealed large pores in the coating and also at the interface, and superficial unevenness of coatings due to internal bubbles. Lee et al. [11] applied induction heating to obtain a coating with a single phase structure on a ductile cast iron from the primary mixtures of Ni and Al powder. They found that coating properties and adhesion quality are dependent on heating rate. Cracks at the interface of coating and substrate were observed in samples in lower heating rates. Also, they found pores with different sizes in all coating samples microstructures. Mohammadnezhad et al. [12] obtained nanostructured NiAl coating on carbon steel by using mechanical alloying. In this process, repeated ball-to-substrate collisions

---

* Corresponding author. Tel.: +98 5118805077.
E-mail address: kianirashid@um.ac.ir (A.-R. Kiani-Rashid).

http://dx.doi.org/10.1016/j.apsusc.2015.01.186

caused cold welding of powder particles to a substrate, and formed a coating on the substrate surface. They observed that at higher milling duration of 600 min delamination, porosity, microcracks and peel of already formed coating occurred and the lamellae near the surface were totally fractured.

Spark Plasma Sintering (SPS) has been introduced as an effective densification method to prevent grain growth of components during sintering. In SPS, fast and controlled heating and a short soaking time at sintering temperature makes it possible to control the sintering process and grain growth [13]. Thus, spark plasma sintering process can be an appropriate method to sinter fine powders obtained from mechanical alloying process. So far, few published works are available on coatings fabricated by SPS and much attention has been paid to this process as a fabrication method for new functional graded materials and composite materials. Researchers have reported fabrication of Al_3Ti layer [14] and Al_3Ti/TiB_2 composite on titanium [15], thermal barrier coating systems on superalloy substrates [16,17], Fe_3Al intermetallic compound layers on austenitic stainless steel [18] via SPS as a fast developing method. Singh et al. [19] reported *in situ* synthesis of $TiC/SiC/Ti_3SiC_2$ composite coating on a titanium substrate by spark plasma sintering. They could improve micro-hardness of the substrate by coating application on it.

In the current research, fabrication of $NiAl/Al_2O_3$ nanostructured composite coatings by SPS technique was studied. To investigate the influence of the reactivity of raw materials on coating process, two different milling times for the powders were applied prior to SPS. So after the ball milling step, a mechanically activated and a reacted powder were obtained and used as raw materials for SPS coating process. The influence of ball milling time of powder and its affinity to undergo an exothermic reaction during heating in SPS on the microstructure, Vickers hardness and scratch resistance of final coating products were investigated.

2. Material and methods

Starting powders for coating were Al (Merck-art no.1056), Ni (Merck-art no.12277) and NiO (Merck-art no.6723) powders. The substrate was nodular, gray cast-iron substrates of SiMo51.

The substrates were cut into disks with diameter of 12 mm and thickness of 2 mm. The chemical composition of SiMo51 substrate can be seen in Table 1.

Starting powders were weighed according to 8Ni + 3NiO + 13Al molar composition to obtain a total of 5.87 g of powder mixture. Ball milling of mentioned powder mixture was carried out in a Retsch planetary ball mill with the ball-to-powder ratio of 10:1, using stainless steel vial and WC balls. To avoid oxidation and excessive cold welding of powders to vial and balls, stearic acid (1 wt.% of the powder mixture) was used as a process controlling agent (PCA). Milling was performed for 1 h and 10 h at 280 rpm. Temperature measurements of the outer wall of the ball mill vial by using RoHS thermochromic liquid-crystal reversible temperature-indicating strip had previously shown that the exothermic reaction in the powder mixture occurred in approximately 100–110 min time range of ball milling [20].

0.3 g of as-milled powder mixture was placed on the substrate surface placed on top of the lower graphite punch in the graphite die with a diameter of 12 mm before cold pressing. Substrates were polished with 3 μm and 1 μm diamond pastes manually. Then the graphite die was fixed in an SPS apparatus (DR. SINTER_ SPS-2050 systems, Fuji Electronic Industrial Co., Ltd, Tokyo, Japan). Coating samples were automatically heated in vacuum from room temperature to 700 °C in 12 min. Then, they were subjected to further heating, at a rate of 50 °C/min, to 1050 °C and held there for 15 min before quenching. It should be mentioned that 3 min after reaching the soaking temperature, a constant uniaxial pressure of 65 MPa was applied and maintained during the rest of the soaking.

Phase evolution of samples was analyzed by PANalytical X'pert PRO XRD, using Cu Kα radiation with λ = 0.15406 nm. Scherrer's equation was used to evaluate the crystallite size of phases in the powder and coating samples from the peak broadening of XRD patterns,

$$D = \frac{0.9\lambda}{\beta \cos \theta} \tag{1}$$

where D is the mean crystallite size, θ is the Bragg angle, λ is the wavelength of the radiation employed, and β is the diffraction peak width at half maximum intensity. Differential thermal analysis (DTA) measurements were carried out in a TG-DTA 1600 Labsys unit within the temperature range 20–1300 °C, applying the heating rate of 40 °C/min. For microstructural observations of powders, a small amount of powder was mounted. The cross section of powder particles was prepared by conventional metallographic techniques. Coating samples were cut for cross sectional microscopic observations, mounted and polished with 3 and 1 μm diamond pastes. It is important to note that while cutting samples, none of the coatings were detached from substrates resulting in good adhesion between coating and substrate. Microstructures and chemical composition of different phases in powders and coating-substrate couples were studied employing a scanning electron microscope (SEM – LEO 1530) with an energy dispersive spectrometer (EDS). In addition to scanning electron microscopy, optical microscopy was utilized to microstructural investigations of the samples. For this purpose, the samples were etched for 6 s in 4 vol.% Nital.

Hardness measurements were performed by Qness-Q10+ Vickers hardness indenter. Because of differences in size and hardness of the different layers, different loads were applied during cross-sectional hardness measurements. For the cast iron substrates HV10, for coatings HV1 and for bond layers, at the interface between coatings and substrates, HV0.001 were measured. In all cases the load was applied for 10 s. The diameter of indenter traces were measured in the indenter instrument, except for the bond layer where diameters of indenter traces were measured by observations in the SEM. For substrates and coatings, the average values of at least 10 hardness measurements were reported, but for the thin bond layers, averages of five points were reported. An average of at least 10 hardness measurements for substrates and coatings and five measurements for bond layers were reported as hardness values.

Since the scratch hardness testing is an indicator of coating cohesion [21], the scratch test was carried out according to ASTM-G171 standard on the surface of the coatings and as-machined substrates by a Parsa Sharif scratch apparatus. Scratch load was 20 N which was kept constant during the test. Scratching speed was 10 mm/min and was also kept constant for all samples. A scratch of length 6 mm was produced during each test. Scratch width were

Table 1
Elemental composition of SiMo51 substrate.

Element	C	Si	Mn	Cr	Ni	Mo	P	S	Mg	Fe
Weight percent	3.17	4.15	0.4	0.1	0.04	0.86	0.02	0.02	0.04	Rest

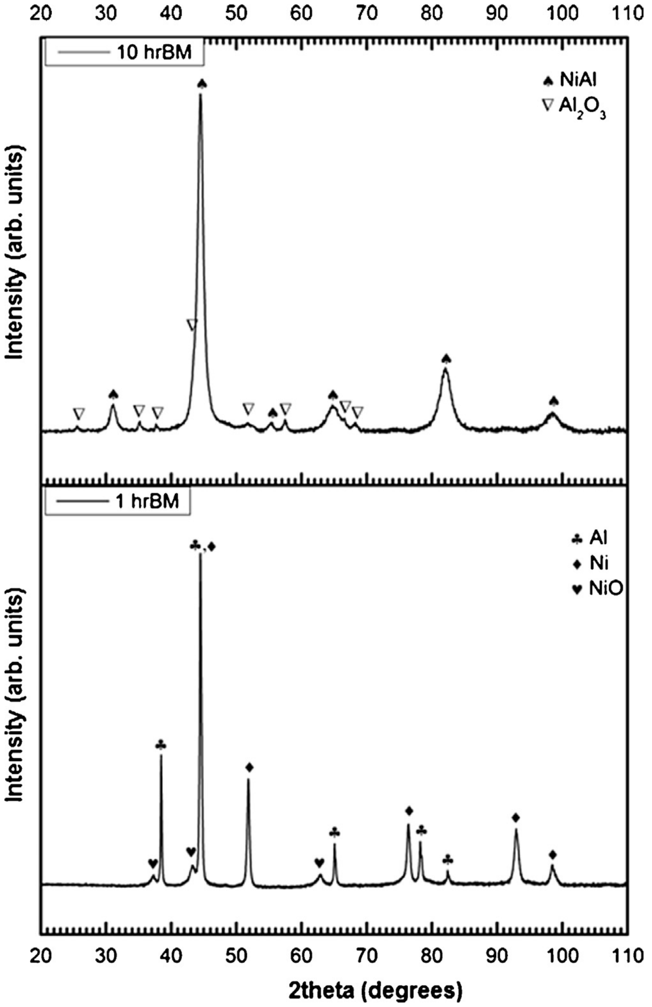

Fig. 1. XRD patterns of powder mixtures after 1 h and after 10 h of ball milling.

measured from images taken by OM and converted to scratch hardness H_s using Eq. (2).

$$H_s = \frac{8F}{\pi W^2} \tag{2}$$

where H_s is scratch hardness based on the scratch width measurement (MPa), F is the applied load (N) and W is the scratch width (mm).

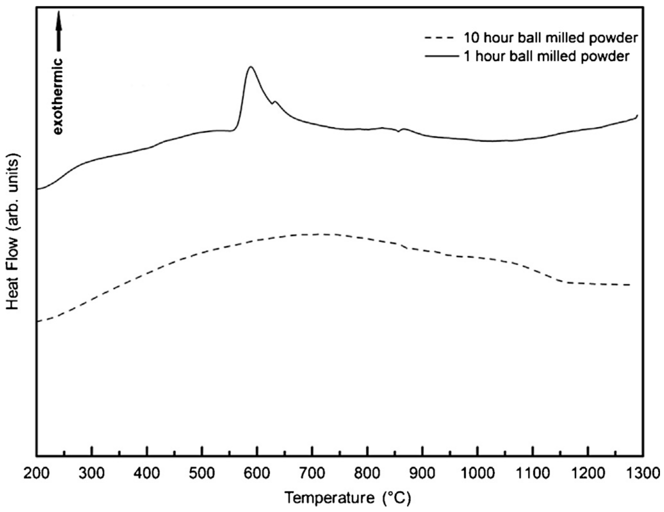

Fig. 3. DTA curves of 1 h and 10 h ball milled powder, heated to 1300 °C with a heating rate of 40 °C/min.

3. Results and discussion

3.1. Powders

In Fig. 1, XRD patterns for powders ball milled for 1 h and 10 h are presented. It is observed that in 1 h ball milled powder, there were just reactant phases and actually none of reaction products were formed during ball milling. Thus, by ball milling for 1 h, mechanical activation of the powder is achieved. However, in 10 h ball milled powder, reaction had happened in ball mill vial and no traces of reactants phases were observed. Crystallite sizes of NiAl and Al_2O_3 after 10 h of ball milling were 9 nm and 17 nm, respectively.

SEM micrographs of powder particles after 1 h and 10 h of ball milling are presented in Fig. 2. It is observed that in powder ball milled for 1 h, mechanical mixing of raw materials happened, while there are some regions which still consisted of one phase. EDS analysis showed that white areas are composed of nickel, dark gray areas are composed of aluminum and in other areas encapsulating of NiO and Ni in softer Al particles has happened extensively. After 10 h of ball milling, microstructure shows a mixture of two phases which EDS analysis results indicated that light gray regions are composed of NiAl and fine dark gray particles have Al_2O_3 composition. So, formation of reaction products is confirmed by microstructural observations, too.

Through the study of powder reactivity, the possibility of reaction happening during the following SPS heat treatment step should be determined. In Fig. 3, the DTA results of the ball milled powders using heating rate of 40 °C/min are shown. In DTA curve of 1 h

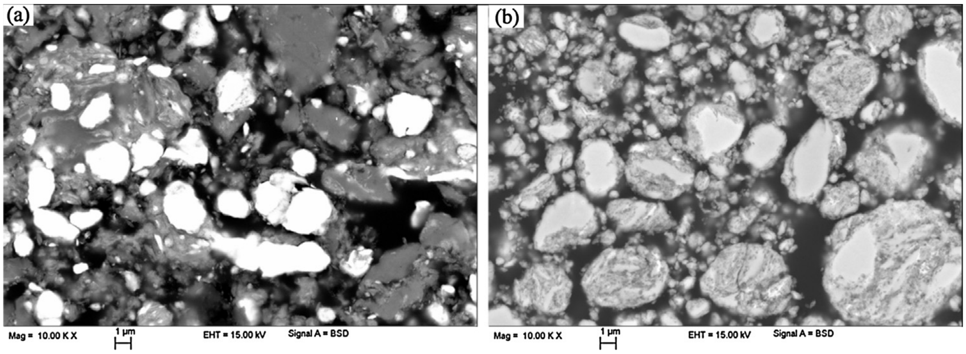

Fig. 2. Cross sectional microstructure images of powder particles after: (a) 1 h and (b) 10 h of ball milling.

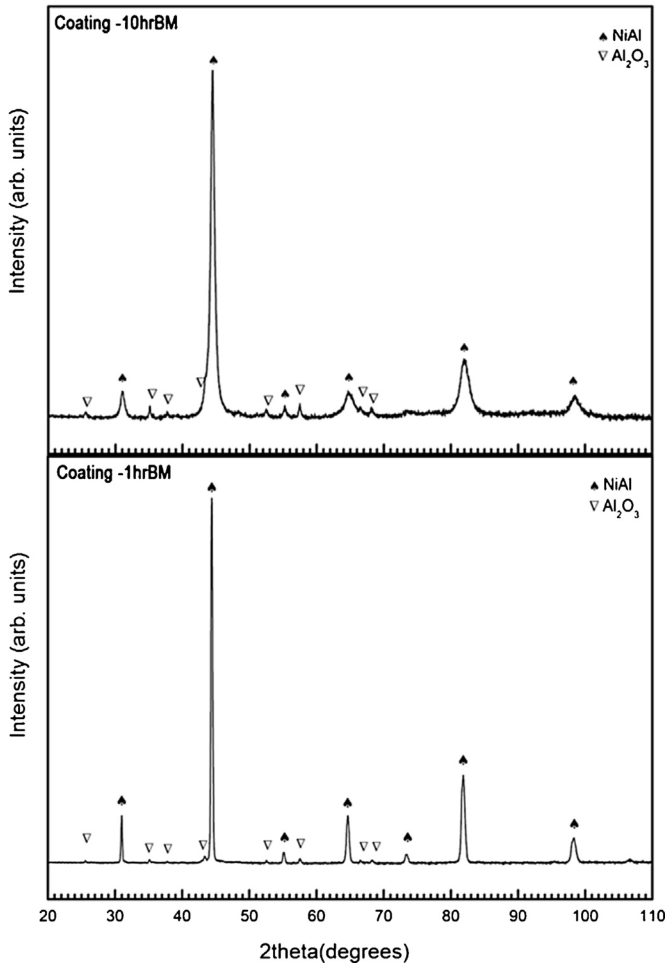

Fig. 4. XRD pattern of coatings made of 1 h and 10 h ball milled powder after SPS.

ball milled powder, there are two exothermic peaks around 580 °C and 630 °C which are related to solid state reaction between NiO and Al and formation of nickel-aluminides, respectively [22]. The endothermic peak at 855 °C, according to Ni–Al phase diagram, corresponds to melting of Al_3Ni formed in the system. But, it can be observed that no thermal events happened in the powder after 10 h of ball milling and the powder did not have any affinity to have a reaction.

Based on the XRD and DTA results of the powders, it can be expected that a reaction would happen in mechanically activated 1 h ball milled powder during the following SPS step, while no reaction would happen in 10 h ball milled powder.

3.2. *Coating samples fabricated by SPS*

Since the enthalpy of reaction between 8 mol of Ni, 3 mol of NiO and 13 mol of Al is −2259 kJ, it is expected that by formation of products a huge amount of heat would be generated.

XRD pattern for coatings made of 1 h and 10 h ball milled powder is shown in Fig. 4. It demonstrates that the reaction was completed by the applied SPS program and *in situ* synthesis of $NiAl/Al_2O_3$ composite coating was fulfilled.

As it was expected, coating made of 10 h ball milled powder consisted of NiAl and Al_2O_3, derived from 10 h ball milled powder. Crystallite sizes of NiAl and Al_2O_3 in coating layer made of 10 h ball milled powder determined by the Scherrer method were 53 nm and 65 nm. Thus, nanostructured composite coating was achieved by using 10 h ball milled powder.

Microstructure (SEM – backscattered imaging) of coating-substrate couples made of 1 h and 10 h ball milled powder can be seen in Fig. 5. EDS analyses in coatings showed that light gray and dark gray grains are composed of NiAl and Al_2O_3, respectively. It can be seen that in the sample made of 10 h ball milled powder nano- to submicron-size alumina particles have been dispersed homogenously in NiAl matrix. Also, it showed both NiAl and alumina had smaller particle size than in the coating sample made of 1 h ball milled powder. Finer and more homogenous microstructure in coating made of 10 h ball milled powder is derived from 10 h ball milled powder (Fig. 2(b)) used as raw material for SPS. In 10 h ball milled powder, products phases were formed during ball milling and they underwent better dispersion in each other by consecutive impacts of balls on powder particles by progressing in ball milling time. In the coating fabricated from 1 h ball milled powder, the occurrence of *in situ* synthesis of phases and coating process simultaneously did not provide any opportunity to product phases for better dispersion in each other.

As it can be observed well in both coating samples, coating layer showed good adherence to the substrate at their interface without any pores or cracks. In both coating samples, there is a diffusion bond layer formed at the coating-substrate interface. The diffusion bond layer in the sample made of 10 h ball milled powder is around 1 μm. It is much thinner than the bond layer in the sample made of mechanically activated powder which is around 5 μm thick. Since the heating program and pressure in SPS were the same for both samples, the reason of this difference lies in another parameter. As it was confirmed above, because the powders used for synthesizing these coatings have different ball milling time, they have different affinity to have reaction. One hour ball milled powder underwent a highly exothermic reaction and the products were formed and coated via combustion synthesis in one step. The heat liberated from the reaction facilitated diffusion of atoms through the interface. So, this system underwent heating by exothermic reaction in addition to SPS instrument heating. But in the sample made of 10 h ball milled powder, products had been synthesized in the ball milling step and thus no exothermic reaction happened during the following SPS process. So, this system underwent heating just by SPS thermal program. More heat experienced by coating sample made of 1 h mechanically activated powder, resulted in more diffusion of atoms through the coating-substrate interface and thus forming a thicker diffusion bond layer than in the coating sample made of 10 h ball milled powder.

To investigate presence of porosity in the coatings, secondary electron imaging on the cross section of the coatings was performed. Figs. 6 and 7 correspond to coating samples made of 1 h and 10 h ball milled powder, respectively. In SE images of both samples, there are dark and bright regions. It was observed that when the contrast of the SE-image was high, a phase with a low mean atomic number showed up in dark color whereas the heavier phase was bright. This contrast is related to the SE detector-signal which selects different energies from different phases, emitted from different depth of the sample. When dark areas, containing the lighter materials, were highlighted in less contrast, brighter areas containing heavier materials showed up, proving that there are not any pores in dark areas. EDS analysis confirmed that darker areas are composed of Al_2O_3 and brighter areas are composed of NiAl. Thus, by microstructural observations no porosity was detected in any of the coatings. It is concluded that SPS process is an applicable method to achieve dense coatings.

Fig. 8 shows an optical micrograph of cross section of sample with coating made of 1 h ball milled powder which was etched in Nital. SiMo51, used as the substrate in this work, is a gray cast iron composed of ferrite and spherical graphite nodules. It is interesting to see that martensite needles were formed in the SiMo51 substrate. While heating SiMO51 to SPS maximum temperature,

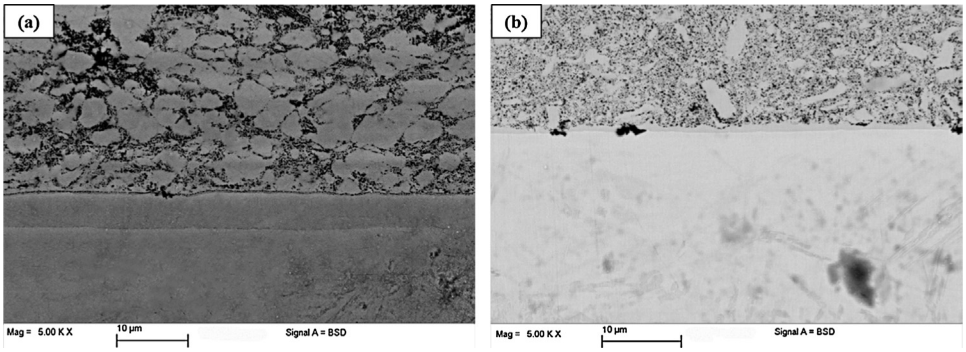

Fig. 5. Backscattered electron SEM imaging on cross section of coating-substrate couples with different layers, from up to bottom, coating, bond layer and substrate; coating made of (a) 1 h, (b) 10 h ball milled powder.

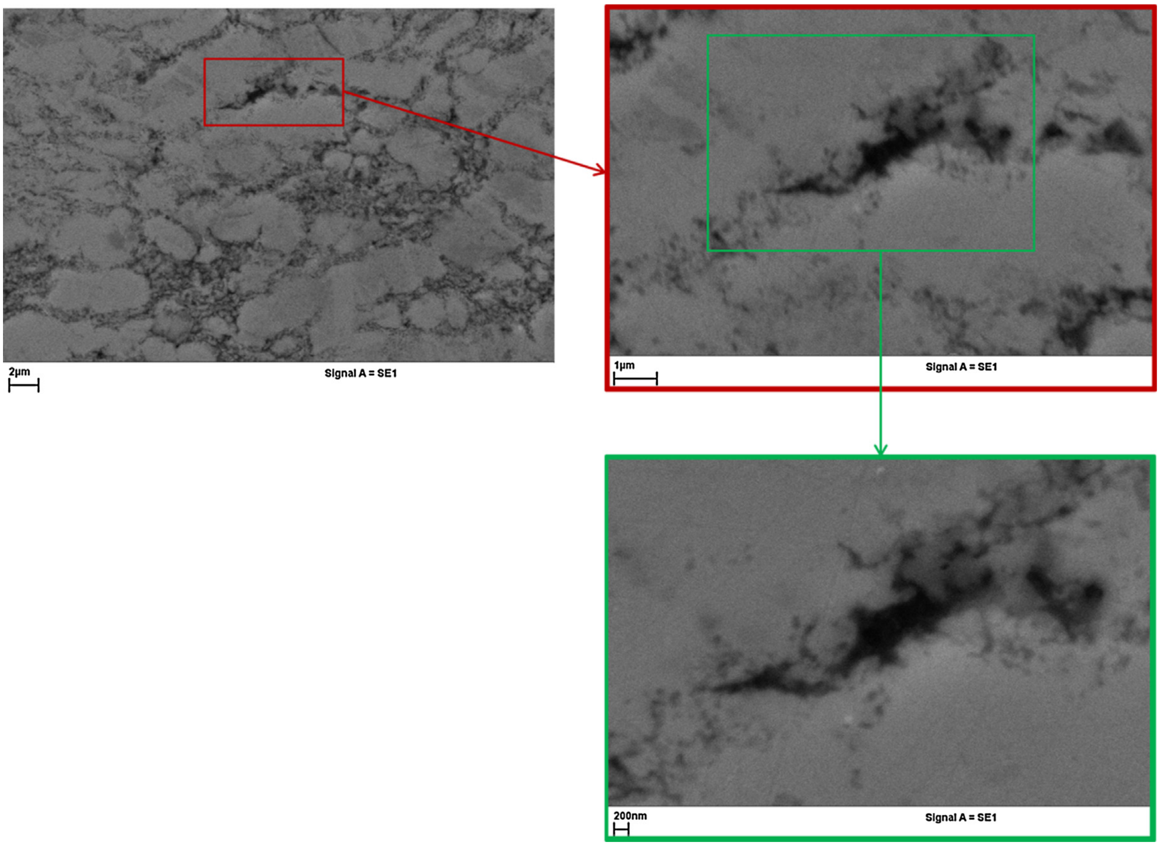

Fig. 6. Secondary electron imaging on the cross section of coating made of 1 h ball milled powder.

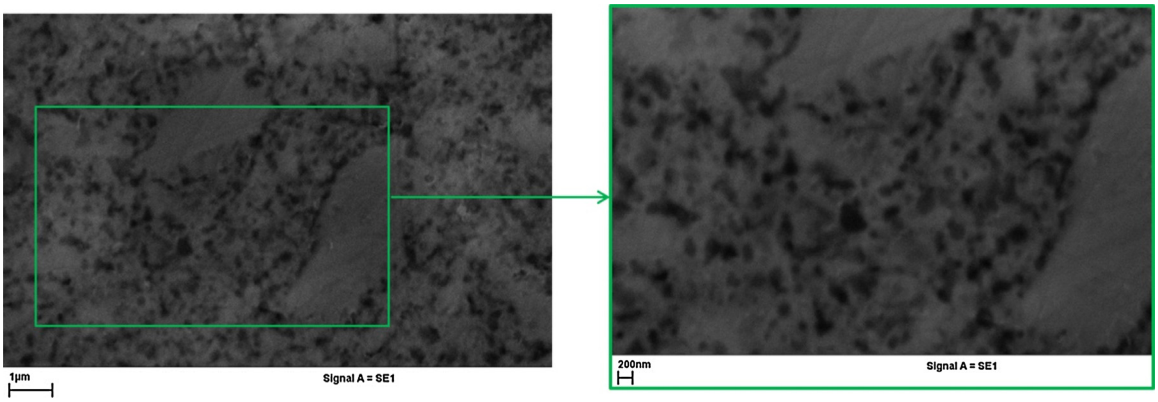

Fig. 7. Secondary electron imaging on the cross section of coating made of 10 h ball milled powder.

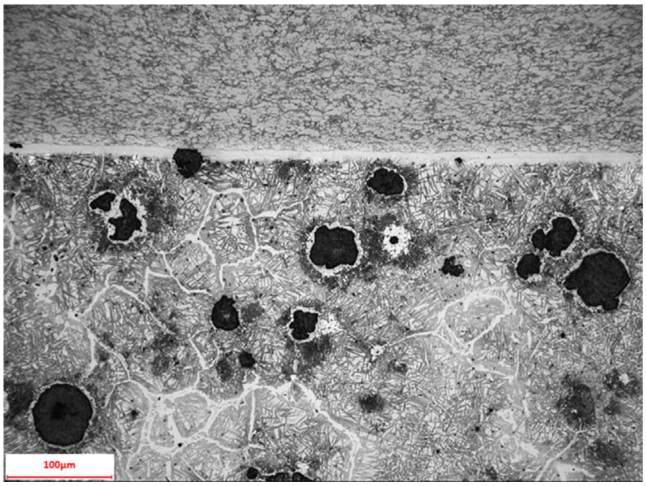

Fig. 8. Optical micrograph of the cross section of the three layers in coating sample made of 1 h ball milled powder, from up to bottom, coating, bond layer and substrate. The sample was etched in Nital 4 vol.% for 6 s.

ferrite to austenite transformation occurred and in the cooling step the austenitic matrix transformed partially to martensite [23]. At the end, a matrix with retained austenite between the martensite needles and the graphite nodules surrounded by ferrite phase is observed in the gray cast iron substrate. Martensitic transformation results in volume increment and so imparts tensile stresses to the interface and the coating. Nevertheless, no cracks or pores were present in the interface which showed that the coating and the interface were tough enough to endure even a martensitic transformation in the substrate. As noted before, coatings did not either cut off from substrate or crack at the interface in any of samples even during cutting in sample preparation step owing to good adhesion. It is interesting to note that graphite nodules could be in contact with the coating layer without reacting with the NiAl–Al_2O_3 composite coating or changing the microstructure in the coating. Also, it seems that the bond layer, i.e., the bright layer in Fig. 8, was formed only in the substrate.

The results of line analysis by EDS across the bond layer of the coating layer and the substrate with the corresponding SEM micrographs are presented in Figs. 9 and 10 for samples with coatings made of 1 h and 10 h ball milled powder, respectively. As can be observed, diffusion of iron and silicon atoms from the cast iron substrate into the coating and nickel and aluminum atoms from the coating to the substrate happened in both samples. It seems that in both samples, bond layer is free of internal stresses, and concentration of these elements alters smoothly in it. So, there is apparently a single phase in the bond layer with large solubility range for Fe, Ni, Si and Al. In the sample with coating made of 1 h ball milled powder the compositions changes linearly from $Fe_{0.65}Si_{0.06}Ni_{0.11}Al_{0.18}$ to $Fe_{0.56}Si_{0.06}Ni_{0.16}Al_{0.22}$ in the bond layer. If the Si content is neglected, the composition varies from $Fe_{0.69}Ni_{0.12}Al_{0.19}$ to $Fe_{0.59}Ni_{0.17}Al_{0.24}$. According to the isothermal section at 1050 °C for the Fe–Ni–Al system presented by Eleno et al. [24], both points fall in the ordered bcc-B2 phase which occupies most of the central portion of the Fe–Ni–Al diagram at that temperature. As the isothermal section only shows the situation at one temperature, it is interesting to compare the compositions with the pseudo-binary Fe–NiAl phase diagram which was also presented by Eleno et al. [24]. In order to do so, the compositions are converted to components of Fe, NiAl and Ni resulting in compositions of $Al_{0.09}(NiAl)_{0.13}Fe_{0.78}$ and $Al_{0.08}(NiAl)_{0.21}Fe_{0.71}$, respectively. In the sample made from the 10 h ball-milled powder, the bond layer appears as a homogeneous single phase with composition varying from $Fe_{0.78}Si_{0.06}Ni_{0.08}Al_{0.08}$ to $Fe_{0.40}Si_{0.05}Ni_{0.30}Al_{0.25}$. By neglecting Si content, the composition would vary from $Fe_{0.83}Ni_{0.08}Al_{0.08}$ to $Fe_{0.42}Ni_{0.32}Al_{0.26}$. By comparing these compositions with the isothermal section of the Fe–Ni–Al system at 1050 °C [24], it is found that the former falls in the two-phase field between the disordered bcc-A2 and fcc-A1 phases and that the latter falls in the ordered bcc-B2 phase. As mentioned above, to use pseudo-binary Fe–NiAl phase diagram, the compositions are converted to $(NiAl)_{0.09}Fe_{0.91}$ and $Ni_{0.08}(NiAl)_{0.35}Fe_{0.57}$, respectively. The comparison shows that the former composition practically falls on the $\gamma/(\gamma+\alpha)$ phase boundary at 1050 °C, that γ transforms to α during cooling and that the composition ends up in the B2 + α two phase field below 600 °C, which is also where the latter composition ends. One may conclude that the NiAl side of the bond layers has an ordered B2-(Fe,Ni)Al phase, then depending on the excess of Al (1 h ball milled) or Ni (10 h ball milled), several things may happen when the Fe-rich side is approached. In excess of Al, the B2-(Fe,Ni)Al phase loses its ordering at about 65% Fe and transforms into disordered α-Fe (i.e., ferrite) and no disordered γ-Fe (austenite) is formed. In excess of Ni, disordered γ-Fe is formed which transforms to α-Fe during cooling. However, as Si, being neglected in the discussion, is a strong α-Fe stabilizer, one may not need to form γ-Fe in the experiments. As the bond layer is cooled it ends up in a miscibility gap with one ordered side, B2, and a disordered side, α-Fe. Probably the rapid cooling from the sintering temperature suppresses this phase separation effectively preserving a homogenous bond layer to room temperature.

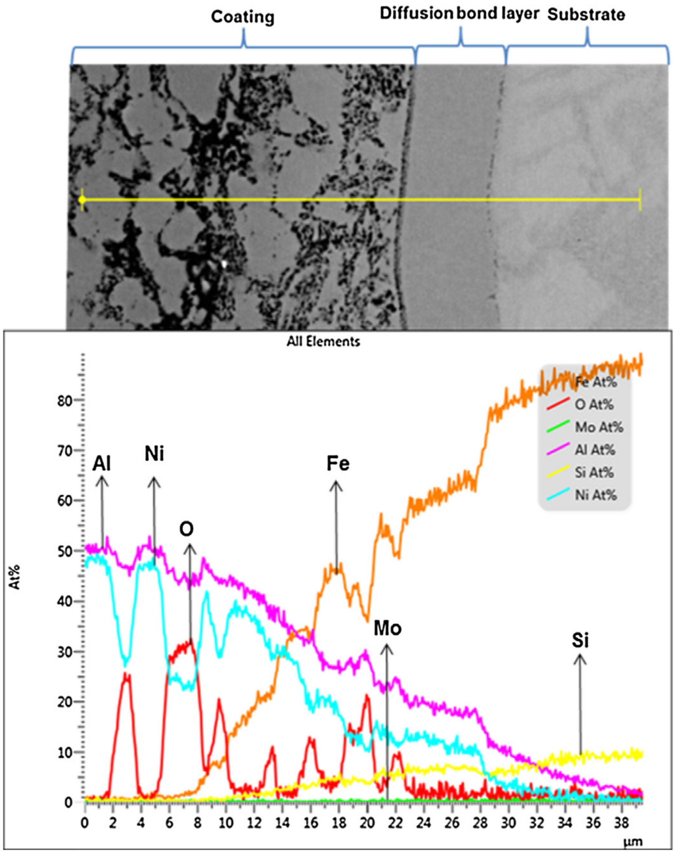

Fig. 9. EDS line scan result for coating sample made of 1 h ball milled powder along the line shown in micrograph.

To investigate the diffusion inside the coating, the amount of free Al was calculated by assuming that all O combined with Al to form Al_2O_3 according to EDS line scan results reported in Figs. 9 and 10. The results for the matrix composition of samples are shown in Fig. 11. By comparison of matrix composition of substrates in both coating samples, it is observed that Ni and Al concentrations in the

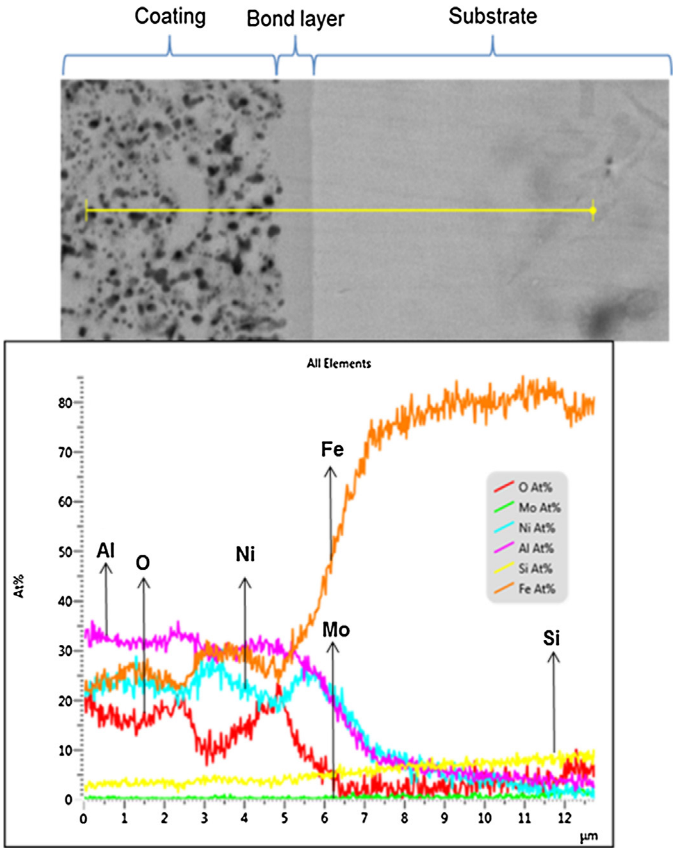

Fig. 10. EDS line scan result for coating sample made of 10 h ball milled powder along the line shown in micrograph.

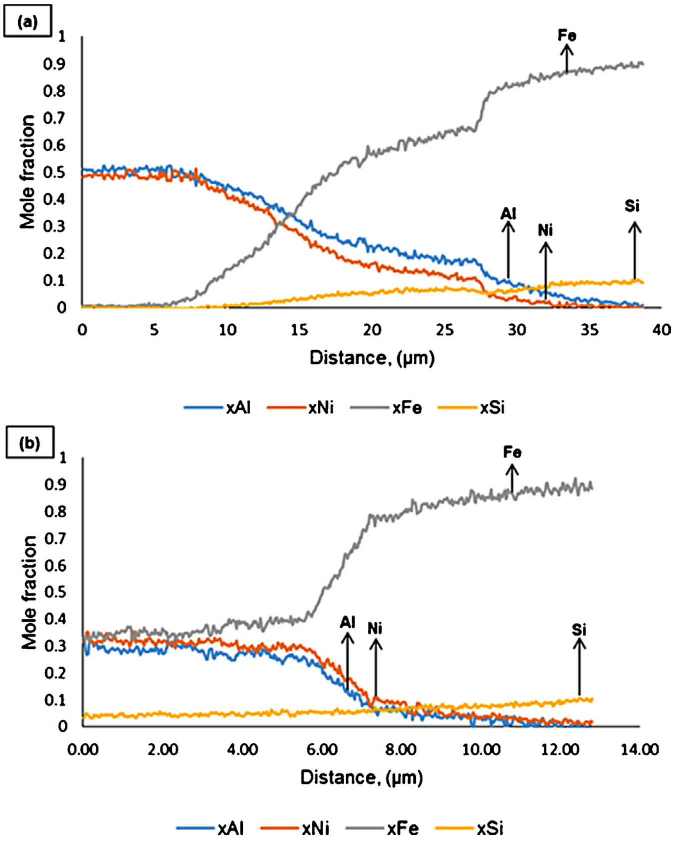

Fig. 11. Matrix composition of sample with coating made of (a) 1 h ball milled powder, (b) 10 h ball milled powder, corresponding to EDS line analysis across the bond layer reported in Figs. 9 and 10.

substrate of sample with coating made of 1 h ball milled powder decreases faster and reaches to zero. In the sample made of 1 h ball milled powder, an exothermic reaction happened in the coating layer. The liberated heat was able to supply the activation energy for formation Fe–Al–Ni intermetallics in its bond layer. So, in this sample, nickel and aluminum were consumed more in the bond layer. It resulted in less concentration of Ni and Al in the substrate of sample made of 1 h ball milled powder than the sample made of 10 h ball milled powder.

The HV1 results for coating in sample made of 1 h and 10 h powder were 490 ± 23 and 646 ± 7 respectively. Dispersion in hardness values for coatings is reasonable. Since coatings consisted of NiAl matrix and Al_2O_3 as the dispersed phase, it was expected to obtain lower hardness when the indenter went into areas richer in NiAl particles and higher values when it went into areas richer in Al_2O_3. In the coating layer of the sample made of 10 h ball milled powder, the value of mean hardness was higher and deviation from the mean value was less than with the sample made of 1 h ball milled powder. This difference can be attributed to finer and more homogenous microstructure in coating made of 10 h ball milled powder. Also, coating made of 10 h ball milled powder showed smaller crystallites. In this microstructure, dislocation motions would be impeded by grain boundaries and homogenously dispersed alumina particles more than coating made of 1 h ball milled powder, resulted in a higher hardness value. HV0.001 could be measured in the bond layer in the sample made of 1 h ball milled powder and the result was 465 ± 12. Since the samples made of 10 h ball milled powder did not show a bond layer that was sufficiently thick, it was not possible to measure hardness without interferences from coating and substrate layers. HV1 measurements on substrates showed comparatively similar results for sample made of 1 h and 10 h ball milled powder as 447 ± 10 and 446 ± 13 respectively. As it can be seen, hardness results showed increasing from the substrates (to the bond layer) to the coating layer.

Scratch hardness of the $NiAl/Al_2O_3$ composite coatings and the substrate was investigated by performing scratch tests on the surface of the samples. In the scratch test, a hard indenter moves under a certain load relative to the material surface at a certain speed. In fact, scratch hardness value indicates the solid surface's ability to resist mechanically induced surface damage or permanent plastic deformation due to friction from a sharp object of a given load and at a sliding speed [21]. The results of scratch test are presented in Fig. 12. It can be concluded that by applying a $NiAl/Al_2O_3$ nanocomposite coating layer, scratch resistance of the cast iron substrate is improved. According to this figure, coating

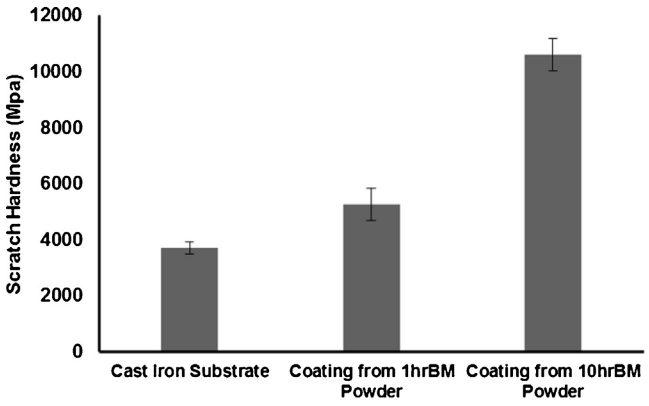

Fig. 12. Scratch hardness of as-machined substrate and coating samples.

made of 10 h ball milled powder shows a pronounced increase in scratch resistance. In fact, this might be because in coating made of 10 h ball milled powder, better dispersion of the alumina particles as the reinforcement phase in NiAl matrix than coating fabricated from 1 h ball milled powder imparts greater frictional resistance to movement of the indenter and so less plastic deformation happens. Also, less crystallite size and thus more grain boundary area of NiAl in coating made of 10 h ball milled powder impedes dislocation motion and improves strength of the NiAl matrix. Scratched surface of coatings did not reveal any cracking or peeling off at coating-substrate interface indicating their good adherence under the test conditions. It is the most interesting observation during scratch testing.

4. Conclusions

This paper investigates effect of powder reactivity on fabrication and properties of NiAl/Al_2O_3 composite coatings on cast iron substrate by spark plasma sintering. The following conclusions can be derived from experiments:

- Ball milling of powder mixtures of Ni, NiO and Al was applied for two different milling times (1 h and 10 h). One hour ball milled powder had only the reactant phases while the 10 h ball milled powder consisted of NiAl and Al_2O_3. Differential thermal analysis results confirmed reactivity of 1 h ball milled powder.
- After SPS, NiAl and Al_2O_3 were observed in coatings made of both reactive and reacted powder mixtures. Microstructural observations demonstrated that the achieved coatings were dense.
- Coating made of 1 h ball milled powder showed a thick, uniform and well-formed diffusion bond layer at the interface between coating and substrate due to the enhancement of atom diffusion by heat liberated from highly exothermic reaction between reactants.
- In bond layers of both samples, concentration of diffusing elements varied smoothly. It seems that a single phase exists in the bond layer.
- No pores or cracks were observed in either coatings or interfaces.
- A finer and more homogenous microstructure in nanostructured coating made of 10 h ball milled powder was observed. It resulted in higher values for mean Vickers hardness and scratch hardness than coating made of 1 h ball milled powder.

Acknowledgements

Authors would like to gratefully acknowledge the financial support provided for this project by Ministry of Science, Research and Technology of Iran. We appreciate Professor Zhijian Shen's extensive help for providing the possibility of samples fabrication with spark plasma sintering apparatus in Department of Materials and Environmental Chemistry (MMK), Stockholm University. Also, we are grateful to Hans Bergqvist, senior researcher at R&D section of SWEREA-KIMAB for his generous scientific support and constant encouragement.

References

[1] M.M. Moshksar, M. Mirzaee, Formation of NiAl intermetallic by gradual and explosive exothermic reaction mechanism during ball milling, Intermetallics 12 (2014) 1361–1366.

[2] H. Zhao, F. Qiu, S. Jin, Q. Jiang, High room-temperature plastic and work-hardening effect of the NiAl-matrix composites reinforced by particulates, Intermetallics 19 (2011) 376–381.

[3] V. Udhayabanu, K.R. Ravi, B.S. Murty, Development of in situ NiAl–Al_2O_3 nanocomposite by reactive milling and spark plasma sintering, J. Alloys Compd. 509S (2011) S223–S228.

[4] V. Udhayabanu, K.R. Ravi, V. Vinod, B.S. Murty, Synthesis of in-situ NiAl–Al_2O_3 nanocomposite by reactive milling and subsequent heat treatment, Intermetallics 18 (2010) 353–358.

[5] G.H. Xu, Z. Lub, K.F. Zhang, The oxidation resistance of submicron-grained NiAl–Al_2O_3 composite fabricated by pulse current auxiliary sintering, Intermetallics 31 (2012) 99–104.

[6] W.W. Lee, D.B. Lee, M.H. Kim, S.C. Ur, High temperature oxidation of an oxide-dispersion strengthened NiAl, Intermetallics 7 (1999) 1361–1366.

[7] N.S. Stoloff, C.T. Liu, S.C. Deevi, Emerging applications of intermetallics, Intermetallics 8 (2000) 1313–1320.

[8] N.P. Padture, M. Gell, E.H. Jordan, Thermal barrier coatings for gas-turbine engine applications, Science 296 (2002) 280–284.

[9] G.P. Cammarota, A. Casagrande, G. Poli, P. Veronesi, Ni–Al–Ti coatings obtained by microwave assisted SHS: effect of annealing on microstructural and mechanical properties, Surf. Coat. Technol. 203 (2009) 1429–1437.

[10] C. Sierra, A.J. Vázquez, NiAl coating on carbon steel with an intermediate Ni gradient layer, Surf. Coat. Technol. 200 (2006) 4383–4388.

[11] H.Y. Lee, A. Ikenaga, S.H. Kim, K.B. Kim, The effects of induction heating rate on properties of Ni–Al based intermetallic compound layer coated on ductile cast iron by combustion synthesis, Intermetallics 15 (2007) 1050–1056.

[12] M. Mohammadnezhad, M. Shamanian, M.H. Enayati, Formation of nanostructured NiAl coating on carbon steel by using mechanical alloying, Appl. Surf. Sci. 263 (2012) 730–736.

[13] M. Eriksson, M. Radwan, Z. Shen, Spark plasma sintering of WC, cemented carbide and functional graded materials, Int. J. Refract. Met. Hard Mater. 36 (2013) 31–37.

[14] T. Matsubara, T. Shibutani, K. Uenishi, K.F. Kobayashi, Fabrication of a thick surface layer of Al_3Ti on Ti substrate by reactive-pulsed electric current sintering, Intermetallics 8 (2000) 815–822.

[15] T. Matsubara, T. Shibutani, K. Uenishi, K.F. Kobayashi, Fabrication of TiB_2 reinforced Al_3Ti composite layer on Ti substrate by reactive-pulsed electric current sintering, Mater. Sci. Eng. A 329–331 (2002) 84–91.

[16] D. Monceau, D. Oquab, C. Estournes, M. Boidot, S. Selezneff, Y. Thebault, Y. Cadoret, Pt-modified Ni aluminides, MCrAlY-base multilayer coatings and TBC systems fabricated by spark plasma sintering for the protection of Ni-base superalloys, Surf. Coat. Technol. 204 (2009) 771–778.

[17] J. Song, K. Ma, L. Zhang, J.M. Schoenung, Simultaneous synthesis by spark plasma sintering of a thermal barrier coating system with a NiCrAlY bond coat, Surf. Coat. Technol. 205 (2010) 1241–1244.

[18] A. Nishimoto, K. Akamatsu, Microstructure and oxidation resistance of Fe_3Al coatings on austenitic stainless steel by spark plasma sintering, Plasma Process. Polym. 6 (2009) S941–S943.

[19] A. Singh, S.R. Bakshi, D.A. Virzi, A.K. Keshri, A. Agarwal, S.P. Harimkar, In-situ synthesis of TiC/SiC/Ti_3SiC_2 composite coatings by spark plasma sintering, Surf. Coat. Technol. 205 (2011) 3840–3846.

[20] M. Beyhaghi, S., Jonsson, A. Kiani-Rashid, M., Kashefi, J. Vahdati Khaki, Unpublished results.

[21] R. Jaworski, L. Pawlowski, F. Roudet, S. Kozerski, F. Petit, Characterization of mechanical properties of suspension plasma sprayed TiO_2 coatings using scratch test, Surf. Coat. Technol. 202 (2008) 2644–2653.

[22] M. Beyhaghi, A. Kiani-Rashid, M. Kashefi, J. Vahdati Khaki, S. Jonsson, Investigation of influences of mechanical activation and heating rate on nanostructured NiAl–Al2O3 composites formation by combustion synthesis, Adv. Process. Mater. Eng. (2015).

[23] M. Ekström, P. Szakalos, S. Jonsson, Influence of Cr and Ni on high-temperature corrosion behavior of ferritic ductile cast iron in air and exhaust gases, Oxid. Met. 80 (2013) 455–466.

[24] L. Eleno, K. Frisk, A. Schneider, Assessment of the Fe–Ni–Al system, Intermetallics 14 (2006) 1276–1290.